

Rapid monocyte kinetics in acute myocardial infarction are sustained by extramedullary monocytopoiesis

Florian Leuschner,¹ Philipp J. Rauch,¹ Takuya Ueno,¹ Rostic Gorbato,¹ Brett Marinelli,¹ Won Woo Lee,^{1,3} Partha Dutta,¹ Ying Wei,⁴ Clinton Robbins,¹ Yoshiko Iwamoto,¹ Brena Sena,¹ Aleksey Chudnovskiy,¹ Peter Panizzi,^{1,5} Edmund Keliher,¹ John M. Higgins,¹ Peter Libby,² Michael A. Moskowitz,⁴ Mikael J. Pittet,¹ Filip K. Swirski,¹ Ralph Weissleder,^{1,6} and Matthias Nahrendorf¹

¹Center for Systems Biology, Massachusetts General Hospital and Harvard Medical School, Simches Research Building, Boston, MA 02114

²Cardiovascular Division, Department of Medicine, Brigham and Women's Hospital, Boston, MA

³Department of Nuclear Medicine, Seoul National University Bundang Hospital, 166 Gumi-ro, Seongnam 463-707, Korea

⁴Stroke and Neurovascular Regulation Laboratory, Massachusetts General Hospital/Harvard Medical School, Charlestown, MA 02129

⁵Department of Pharmacal Sciences, Harrison School of Pharmacy, Auburn University, Auburn, AL 36849

⁶Department of Systems Biology, Harvard medical School, Boston, MA 02115

Monocytes (Mo) and macrophages (MΦ) are emerging therapeutic targets in malignant, cardiovascular, and autoimmune disorders. Targeting of Mo/MΦ and their effector functions without compromising innate immunity's critical defense mechanisms first requires addressing gaps in knowledge about the life cycle of these cells. Here we studied the source, tissue kinetics, and clearance of Mo/MΦ in murine myocardial infarction, a model of acute inflammation after ischemic injury. We found that a) Mo tissue residence time was surprisingly short (20 h); b) Mo recruitment rates were consistently high even days after initiation of inflammation; c) the sustained need of newly made Mo was fostered by extramedullary monocytopoiesis in the spleen; d) splenic monocytopoiesis was regulated by IL-1β; and e) the balance of cell recruitment and local death shifted during resolution of inflammation. Depending on the experimental approach, we measured a 24 h Mo/MΦ exit rate from infarct tissue between 5 and 13% of the tissue cell population. Exited cells were most numerous in the blood, liver, and spleen. Abrogation of extramedullary monocytopoiesis proved deleterious for infarct healing and accelerated the evolution of heart failure. We also detected rapid Mo kinetics in mice with stroke. These findings expand our knowledge of Mo/MΦ flux in acute inflammation and provide the groundwork for novel anti-inflammatory strategies for treating heart failure.

CORRESPONDENCE

Matthias Nahrendorf:
mnahrendorf@mgh.harvard.edu
OR

Ralph Weissleder:
rweissleder@mgh.harvard.edu

Abbreviations used: CT, computed tomography; DTPA, diethylenetriaminepentaacetic acid; FMT, fluorescence molecular tomography; GMP, granulocyte macrophage progenitor; MDP, MΦ dendritic cell progenitor; MI, myocardial infarction; Mo, monocyte; MΦ, macrophage; MPS, mononuclear phagocyte system; SPX, splenectomy; TUNEL, terminal deoxynucleotidyltransferase-mediated dUTP-biotin nick end labeling.

Monocytes (Mo) and the macrophages (MΦ) to which they give rise are key effectors of immune homeostasis and response to injury. Virtually all disease areas with high socioeconomic impact, including cancer, infection, and autoimmune and cardiovascular diseases, share similarities in engagement of the innate immune system. Often, these cells participate integrally in defense and tissue repair mechanisms, yet aberrant Mo/MΦ function, as can occur in atherosclerosis and cancer, may instead aggravate disease. Hence, Mo/MΦ are emerging therapeutic targets in the multitude of disorders that involve inflammation

(Shimura et al., 2000; Libby, 2002; Luo et al., 2006; Moskowitz et al., 2010).

Our knowledge of the mononuclear phagocyte system (MPS) has expanded rapidly (Gordon and Taylor, 2005; Liu et al., 2009; Geissmann et al., 2010). Today, we know that Mo arise from hematopoietic stem cells (HSCs) in the bone marrow, pass through several intermediate

© 2012 Leuschner et al. This article is distributed under the terms of an Attribution-Noncommercial-Share Alike-No Mirror Sites license for the first six months after the publication date (see <http://www.rupress.org/terms>). After six months it is available under a Creative Commons License (Attribution-Noncommercial-Share Alike 3.0 Unported license, as described at <http://creativecommons.org/licenses/by-nc-sa/3.0/>).

progenitor stages (granulocyte M Φ progenitor [GMP] \rightarrow M Φ dendritic cell progenitor [MDP]; Geissmann et al., 2010) and migrate into the blood pool depending on the cytokine receptor CCR2 (Serbina and Pamer, 2006). This developmental program may take up to 1 wk (Johnston, 1988). Mo then circulate in blood and patrol the vasculature (Auffray et al., 2007) for several days, before they are recruited to sites of inflammation where they can give rise to M Φ and Mo-derived DCs (Mo-DCs; Cheong et al., 2010) and pursue a myriad of functions in tissue, including phagocytosis (Gordon and Taylor, 2005), antigen presentation (Cheong et al., 2010), regulation of inflammation, and tissue repair (Geissmann et al., 2010; Robbins and Swirski, 2010). We have recently learned that a splenic reservoir dominates Mo supply in the first 24 h of acute inflammation (Swirski et al., 2009), and that the two major Mo subsets' distinct timing follows specific cytokine cues (Nahrendorf et al., 2007b). Next, we must address critical knowledge gaps in our understanding of the myeloid cell life cycle before we can therapeutically harness the MPS without compromising the organism's defense mechanisms.

In pursuit of such knowledge, we used mice with myocardial infarction (MI) to fate-map Mo/M Φ . Two considerations prompted the choice of this preparation, in which coronary artery ligation causes sterile tissue injury and ischemic necrosis of myocytes. First, coronary ligation in the mouse is a well-studied model of tissue injury in an organ that can be transplanted for fate mapping experiments. Second, MI is the major cause of sudden death and the expanding world-wide heart failure epidemic (National Heart, Blood, and Lung Institute, 2009). Mo/M Φ have emerged as key regulators of infarct healing; they execute essential functions such as removing dead tissue, promoting angiogenesis, and coordinating extracellular matrix

turnover in the acute infarct (Nahrendorf et al., 2010b). Preclinical (Panizzi et al., 2010) and clinical data (Tsujioka et al., 2009; Aoki et al., 2010) suggest that both insufficient and exuberant recruitment of Mo/M Φ are detrimental and may result in infarct expansion, left ventricular dilation, and heart failure.

By tracking Mo/M Φ from birth to death, we discovered that cell flux is surprisingly fast; that the spleen is a major source of Mo beyond its initial reservoir function; that IL-1 β -triggered extramedullary emergency monocytopoiesis contributes substantially to the cell population in the infarct throughout the course of acute inflammation; and that Mo/M Φ can exit inflamed infarct tissue and travel to lymphatic organs and the liver, although local cell death quantitatively dominated cell clearance. Rapid Mo turnover and splenic Mo production were also found in mice with stroke, indicating that the infarct data can be generalized. These findings provide new information on mononuclear phagocyte kinetics during tissue injury, and solidify our knowledge of Mo/M Φ fate in acute inflammation.

RESULTS

Myeloid cells show fast turnover in inflamed tissue

Previous studies have addressed Mo behavior in circulation (van Furth and Cohn, 1968; Issekutz et al., 1981; Tacke et al., 2006); however, less is known about these cell's kinetics once they enter inflamed tissue (Helft et al., 2010). We therefore studied the turnover of Mo and Mo-derived M Φ in MI, an injury that elicits a robust recruitment of Mo and presence of M Φ for the first 1–2 wk (Frangogiannis et al., 2002).

Transplantation of infarcted hearts from CD45.2⁺ mice into CD45.1⁺ recipients, and flow cytometric analysis of digested infarcts at different time points, allowed us to follow dynamic changes in the Mo population at the site of inflammation

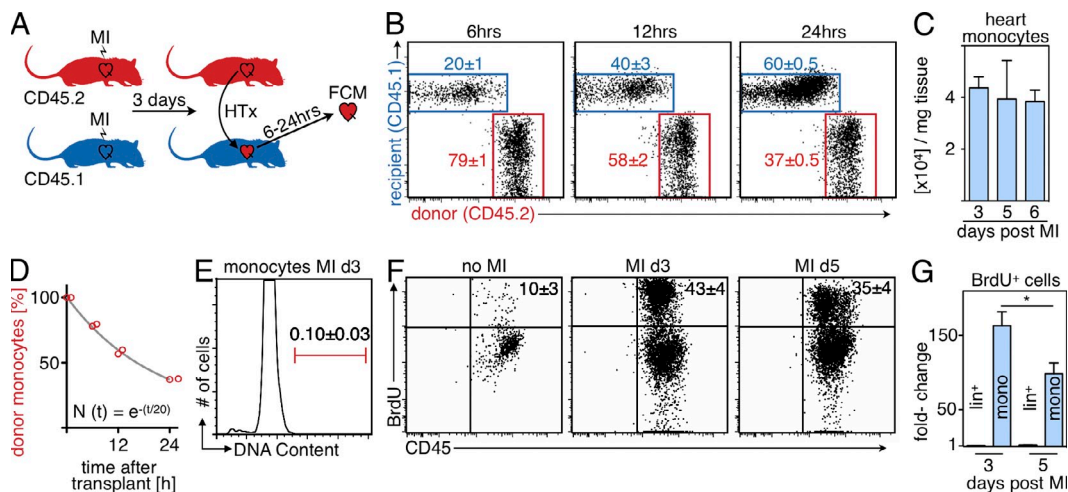


Figure 1. Monocyte infarct residence time after ischemia. Cell tissue kinetics were studied using flow cytometric analysis (FCM) of heart transplants and BrdU pulse experiments. (A) Schematic set-up of the experiment ($n = 16$; experiment was performed four times). (B) Dot plots of FCM analysis showing the contribution of donor- and recipient-derived Mo in the infarcted heart at 6, 12, and 24 h after transplantation of the heart. (C) Number of Mo retrieved from digested infarcts on day 3 to 6 after MI by FCM. (D) Fitting of donor Mo (y-axis) over time (x-axis). Red circles indicate individual data, the gray line represents the fit described by the equation. (E) Flow cytometric DAPI staining of Mo in the infarct on day 3 after coronary ligation. (F) FCM analysis of the infarct 24 h after BrdU pulse. Dot plots are gated on Mo. (G) Fold-change in BrdU⁺ Mo and lineage⁺ cells in the heart after MI. Mean \pm SEM ($n = 3$ –10 per group, experiment was repeated twice). *, $P < 0.05$.

(outlined in Fig. 1 A). Donor and recipient mice were genetically identical except for the surface marker CD45 on white blood cells. The heterotopic heart transplant used in our fate mapping experiments induces a brief additional ischemia; therefore, isograft transplantations of noninfarcted CD45.2⁺ hearts into CD45.1⁺ recipients served as controls. We found that the mean graft ischemia time during transplantation of 15.1 ± 0.9 min resulted in the accumulation of $4 \times 10^3 \pm 10^3$ Mo per mg tissue in isograft controls, whereas the number of Mo on day 4 after MI was $\sim 5 \times 10^4$ per mg infarct tissue, an order of magnitude higher. These control experiments indicate that the transplantation procedure had relatively modest effects on cell kinetics.

Analysis at 6, 12, and 24 h after transplantation of infarcted hearts revealed a rapid decrease of donor-derived Mo in the infarct, and the number of Mo recruited from the recipient increased at a much faster rate than expected. As soon as 6 h after transplantation, $20 \pm 1\%$ of the Mo in the infarct were newly recruited from the recipient mouse. This number increased to $40 \pm 3\%$ at 12 h. After 24 h, the majority ($60 \pm 0.5\%$) of Mo present in the infarct derived from the recipient (Fig. 1 B).

These data informed a mathematical model of MPS dynamics in MI. Absolute leukocyte counts in the infarct remain fairly stable from day 3–6 after MI (Fig. 1 C; Nahrendorf et al., 2007b). The total Mo count was thus assumed to be constant, and we estimated its turnover rate by fitting a mathematical function to the percentage of donor-derived Mo in the MI at different points in time (Fig. 1 D). We found that the size of the donor-derived population was well-approximated by a single exponential decay with a rate of 5% per hour. A least-squares fit between this model and the data had an adjusted R^2 value of $>99\%$. The model suggests that the rate of cellular turnover is roughly constant during this period of time after MI. This turnover rate corresponded to an average residence time of Mo in tissue of 20 h (for a detailed description of the model see the [Supplemental discussion](#)).

We then used BrdU pulse-chase experiments to explore if these unexpectedly fast cell fluxes could be supported with a second, independent method. To this end, we injected mice with BrdU, which incorporates into proliferating DNA in place of thymidine. This method labels cells that divide after the BrdU pulse. Flow cytometric staining for BrdU, at 24 h after the pulse, enumerated Mo that had either proliferated in the infarct or that were recruited from a circulating cell population that was maintained by monocytopoiesis elsewhere. Cell cycle analysis showed that Mo in the infarcted myocardium were not in S or G2 phase (Fig. 1 E), indicating that there was no local proliferation. Another potential source for BrdU⁺ cells in the infarct could be the accumulation of upstream myeloid progenitor cells, which proliferate and give rise to Mo. However, we found an extremely low number of these cells in the infarct (17 ± 6 and 36 ± 4 MDPs in the entire infarct on days 3 and 6 after coronary ligation, respectively). We therefore concluded that all BrdU⁺ Mo were newly

recruited to the site of inflammation after the time of BrdU injection. Analysis of cells retrieved from 3-d-old infarcts revealed that $43 \pm 4\%$ of Mo in the infarct were BrdU⁺, and therefore at least 43% of the Mo were recruited within the preceding 24 h (Fig. 1 F). It is worth noting that only 3% of lineage⁺ cells were BrdU⁺. During phase 2 of infarct healing (5 d after coronary ligation), $35 \pm 4\%$ of Mo in the myocardium stained positively for BrdU. The absolute number of BrdU⁺ Mo in the heart increased >160 -fold on day 3 after MI and by 98-fold on day 5 after MI (Fig. 1 G). In contrast, we did not detect an increase of lineage⁺ cells that incorporated BrdU (Fig. 1 G). Mo subset analysis revealed faster kinetics for inflammatory Ly-6C^{high} when compared with Ly-6C^{low} Mo (Fig. 2). The BrdU data likely underestimate cell recruitment, as they do not include newly recruited cells that proliferated before the injection of BrdU. This consideration may explain why the measurement of newly recruited Mo was 60% in the transplant approach, but only 43% by BrdU labeling. Both methods reveal rapid cell kinetics in acute inflammation, with an average tissue residence time of 20 h.

Local death is the major, and egress a minor, contributor to cell clearance

The Mo/M Φ population swells rapidly after onset of ischemia and starts to shrink 1 wk later during resolution of inflammation. In between, despite the persistent and massive cell recruitment and the short half-life in tissue described above, the size of the population remains fairly constant (Nahrendorf et al., 2007b). As cell clearance should therefore

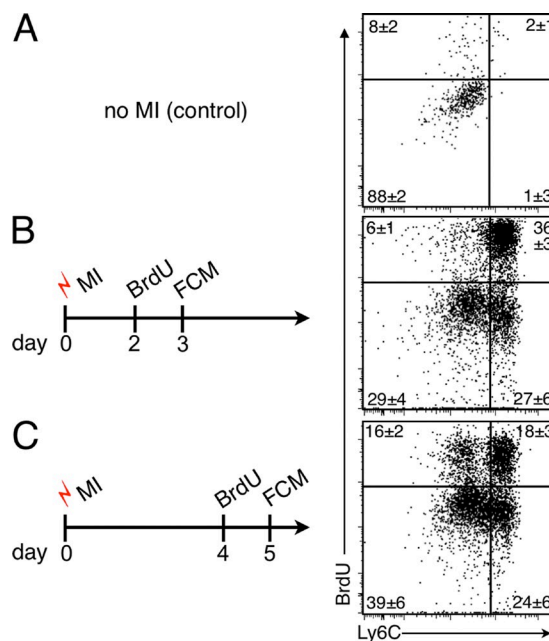


Figure 2. Kinetics of Mo subsets after MI. (A) FCM of BrdU pulse experiment in naive mice on day 3 after MI (B) and on day 5 after MI (C). Dot plots show Mo identified as CD11b^{high} (CD90/B220/CD49b/NK1.1/Ly-6G)^{low} (F4/80/CD11c)^{low}, including separation into subsets using Ly-6C. Mean \pm SEM ($n = 4$ –6 per group, experiment was repeated twice).

match recruitment, we next investigated the relative contribution of three alternatives: (1) Mo/MΦ may exit the site of inflammation and reenter circulation, (2) they may die locally, or (3) both processes may contribute. In this study, we focused on lineage⁻ CD11b⁺ cells because only a small fraction of myeloid cells in the heart was CD11b⁻ ($4.2 \pm 0.7\%$ cells were F4/80⁺ CD11b⁻ and $2.1 \pm 0.2\%$ were CD11c⁺ CD11b⁻ on day 3 after MI).

To investigate cell exit, we first used transplantation of infarcted hearts between mice with diverging CD45 leukocyte surface markers. We transplanted hearts 3 d after MI and collected blood and tissue samples from various organs 24 h later (Fig. 3 A). CD11b⁺ CD45.2⁺ donor cells, which were “transplanted” while residing in the infarcted heart, were detected in the CD45.1⁺ host circulation and destination tissues. Although we clearly encountered cell exit, the numbers were small. Assuming a mouse blood volume of 0.080 ml/g (Mitruka and Rawnsley, 1977), we enumerated $10,388 \pm 3,006$

exited CD45.2⁺ lineage⁻ CD11b⁺ cells in the entire host circulation. The highest number of cells was found in the liver ($12,429 \pm 4,693$), followed by the draining lymph nodes ($3,383 \pm 3,176$) and the spleen (885 ± 592 ; Fig. 3 A). In summary, only 5% of Mo/MΦ present at the site of inflammation were encountered in remote organs 24 h after transplantation. Of note, only F4/80^{low} cells were found to have exited, suggesting that only undifferentiated Mo leave the site of inflammation.

It is possible that exited cells approach the end of their lives and are then rapidly eliminated by scavenging MΦ. Fast clearance of exited cells—and the CD45 surface marker we relied on for detection—may have led to an underestimation of the exit rate. We therefore conceived a second experiment that used a nonbiodegradable cell label. Specifically, we derivatized a nanoparticle that distributes to infarct Mo/MΦ with the slow-decaying radioisotope ¹¹¹Indium via the tight chelator diethylenetriaminepentaacetic acid (DTPA; ¹¹¹In-CLIO). Previous work (Harisinghani et al., 2003;

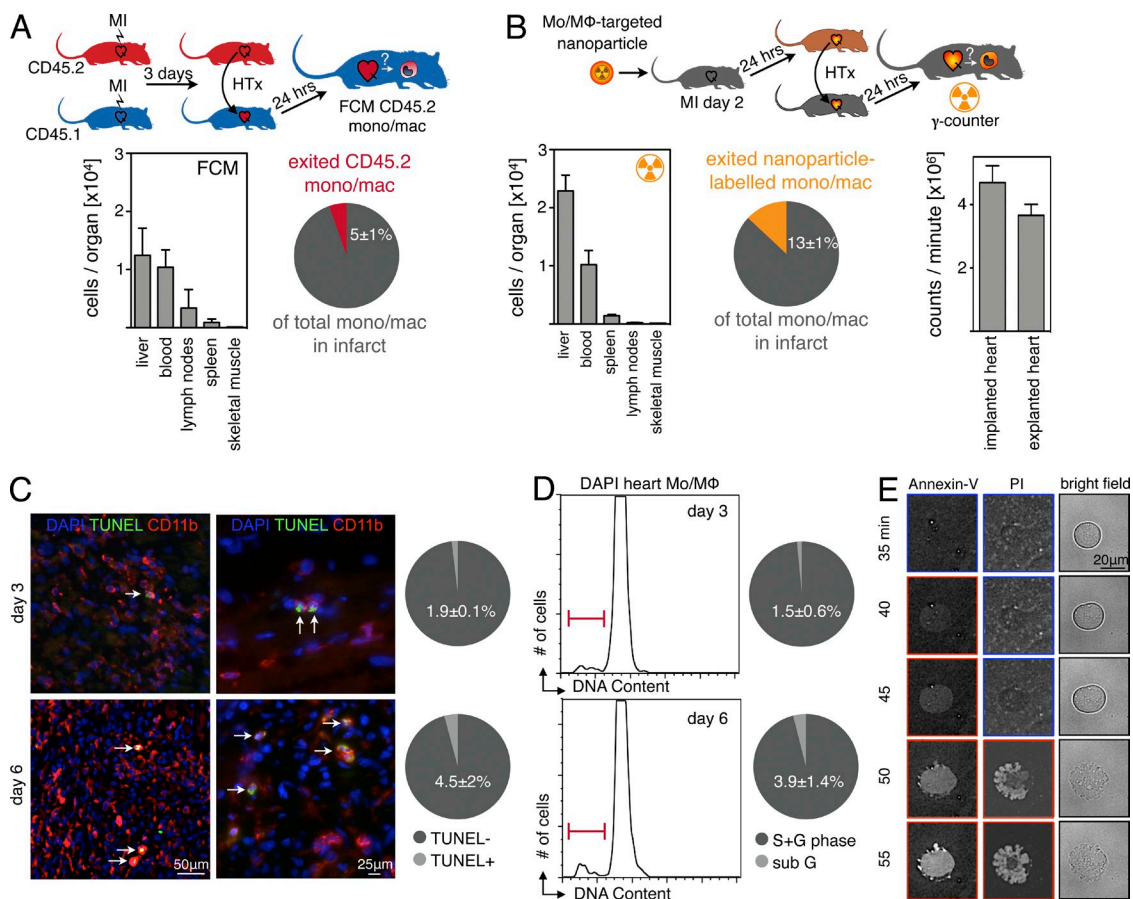


Figure 3. Mo clearance. Cell exit and local death were studied as major contributors to cell clearance from the site of inflammation. (A) Bar graph shows number of exited CD45.2⁺ Mo in organs based on FCM; pie chart illustrates percentage of exited myeloid cells normalized to the number in the infarct ($n = 5$). (B) Left bar graph shows exited cell number in organs calculated using alternative scintillation data; pie chart illustrates the exit rate. The right bar graph reflects decay-corrected photon counts of the graft before and 24 h after heart transplantation. Experiment was done in duplicate, data are mean \pm SEM. (C) Immunofluorescence of infarct tissue (DAPI, blue; TUNEL, green; CD11b, red). Pie charts indicate frequency of TUNEL signal in CD11b⁺ cells (arrows; $n = 5$ per group). (D) Analysis of cell death by DAPI FCM staining in the heart ($n = 4$ per group). (E) In vitro time lapse microscopy of representative splenic Mo to determine timing of cell death signals. Experiment was done in duplicates.

Weissleder et al., 2005; Devaraj et al., 2009; Swirski et al., 2009; Panizzi et al., 2010) and own, unpublished data show that these nanoparticles efficiently label Mo/M Φ and are cleared from the intravascular/extracellular space 24 h after intravenous injection. Mice were injected with ^{111}In -CLIO two days after MI (Fig. 3 B). We then waited 24 h to allow for sufficient uptake into Mo/M Φ in the infarct. Next, the heart containing ^{111}In -CLIO labeled infarct Mo/M Φ was transplanted into a recipient mouse. Before transplantation and after a 24 h period that allowed for exit of labeled cells, the heart was studied by scintillation counting. After correction for ^{111}In decay, we calculated the reduction of ^{111}In -CLIO signal in the graft, and by extension departure of Mo/M Φ from the infarct. We found $46.9 \times 10^5 \pm 5.2 \times 10^5$ gamma counts per heart before implantation and $36.6 \times 10^5 \pm 3.4 \times 10^5$ counts per heart 24 h later (Fig. 3 B). We also measured radioactivity in blood and exiting cell's potential destination organs. Assuming a Mo/M Φ population size of 7×10^5 in MI (Nahrendorf et al., 2007b) and using the activity at time of transplantation, we calculated a photon count per Mo/M Φ value of 5.2, which we then used to estimate the number of exited cells in transplant recipient tissues (Fig. 3 B). We found that the liver and blood were the compartments with the highest numbers of exited Mo/M Φ ($22,903 \pm 2711$ and $10,220 \pm 2410$, respectively), confirming the results obtained with flow cytometric detection of CD45.2. Summing radioactivity measured in the transplant recipient, we calculated that 13% of Mo/M Φ had exited the heart within 24 h. We thus concluded that while exit occurred, its contribution to Mo/M Φ clearance from the site of acute inflammation was minor.

Recruited innate immune cells can undergo apoptosis in MI in rabbits (Takemura et al., 1998). We therefore studied the rate of local Mo/M Φ death in acute inflammation. We co-stained hearts harvested from mice 3 and 6 d after MI for CD11b, a surface marker for myeloid cells, and terminal deoxynucleotidyltransferase-mediated dUTP-biotin nick end labeling (TUNEL; Fig. 3 C). TUNEL staining in infarcts harvested from CX3CR1^{flp/+} mice confirmed that TUNEL⁺ cells were Mo and not neutrophils (unpublished data). Quantification revealed that $1.9 \pm 0.1\%$ of CD11b⁺ cells were also TUNEL⁺, and therefore were undergoing apoptosis. On day 6 after MI, when the Mo/M Φ population begins to contract, $4.5 \pm 2.0\%$ of Mo/M Φ were TUNEL⁺ (Fig. 3 C, MI day 3 vs. MI day 6; $P = 0.03$).

To evaluate these results with a second, independent method, we analyzed Mo/M Φ retrieved from infarcts by flow cytometric staining for DAPI. On day 3 after MI, $1.5 \pm 0.6\%$ of Mo/M Φ were in sub-G-phase, indicating apoptosis (Darzynkiewicz et al., 1992). On day 6 after MI, $3.9 \pm 1.4\%$ showed a sub-G expression (MI day 3 vs. MI day 6; $P = 0.04$). Similar results were obtained by flow cytometric analysis of active caspase 3 (Fig. 3 D, MI day 3, $2.3 \pm 0.42\%$ versus day 6, $4.5 \pm 0.38\%$, $P < 0.05$), thus confirming these apoptotic rates.

Histological and flow cytometric staining for death markers provided us only with an instantaneous “snap shot,” i.e., we

learned how many cells were dying at the time of sacrifice. Yet, comparison of death to recruitment rates requires calculation of how many cells die locally within 24 h, and thus consideration of the duration of cell death. Previous work reported that apoptosis may take ~ 30 min for fibroblasts (Evan et al., 1992) and from 30 min to 2 h for cardiomyocytes (Guerra et al., 1999). Because timing had not been studied in Mo/M Φ , we cultured splenic Mo/M Φ for dynamic multispectral fluorescence microscopy. During imaging, the cell medium contained fluorescently labeled Annexin V, a marker of early stage apoptosis, and propidium iodide (PI), which indicates late-stage cell death. We found numerous events of cell death in a 2-h time-lapse microscopy experiment. Fig. 3 E shows a representative cell, which was viable for the first 35 min of image acquisition. Annexin V staining of the membrane was detected at 40 min. At this time point, no PI signal was present, but it was detected 10 min later and was accompanied by cell integrity destruction on bright field images. Analyzing 10 fields of view, we found a mean delay of 11 ± 3 min from the onset of Annexin V signal (indicating a cell had entered apoptosis) to onset of PI signal and destruction of the cell on bright field images (indicating completion of the cell death program). The in vitro signal duration of 11 min likely indicates a limited phase of cell death, whereas the complete process of programmed cell death may take longer in vivo (Spencer and Sorger, 2011). Nevertheless, these data provide useful information on the duration of certain “death signals” and allowed us to calculate that $>10^6$ apoptotic events could occur in 24 h, using the measured apoptotic rate of 1.9%, 11 min of death signal, and a population of 0.7×10^6 Mo/M Φ in the infarct. Overall, these results are consistent with a dominant contribution of local death to Mo/M Φ clearance in acute inflammation.

The spleen supplies Mo throughout the duration of acute inflammation

The high rate of Mo recruitment beyond the initial surge after injury raised the question of the source of these cells. The splenic Mo reservoir contributes predominantly to the infarct Mo/M Φ population in the first 24 h after injury (Swirski et al., 2009; Leuschner et al., 2010). After BrdU injection, we observed an increase of BrdU⁺ Mo in the spleen from $19 \pm 4\%$ in the steady state to $56 \pm 4\%$ on day 3 after MI and $47 \pm 8\%$ on day 5 after infarct surgery. We therefore hypothesized that the spleen continues to contribute cells beyond the first 24 h. We removed the spleen on day 5 after MI and studied the Mo/M Φ population in the infarct 24 h later by flow cytometric enumeration. Surprisingly, even at this late time point, removal of the spleen drastically reduced the number of Mo in inflamed tissue (Fig. 4 A; $3.8 \times 10^4 \pm 4 \times 10^3$ vs. $1.3 \times 10^4 \pm 2 \times 10^3$; $P < 0.01$). In bone marrow, Mo did not increase significantly, although Mo numbers in the blood mirrored the reduction in the heart (Fig. 4 A; $3.4 \times 10^5 \pm 8 \times 10^4$ vs. $2 \times 10^5 \pm 2 \times 10^4$; $P < 0.05$). Intriguingly, the number of BrdU⁺ Mo in infarct tissue fell significantly after splenectomy (Fig. 4 B; from $34 \pm 5\%$ to $18 \pm 7\%$; $P < 0.05$).

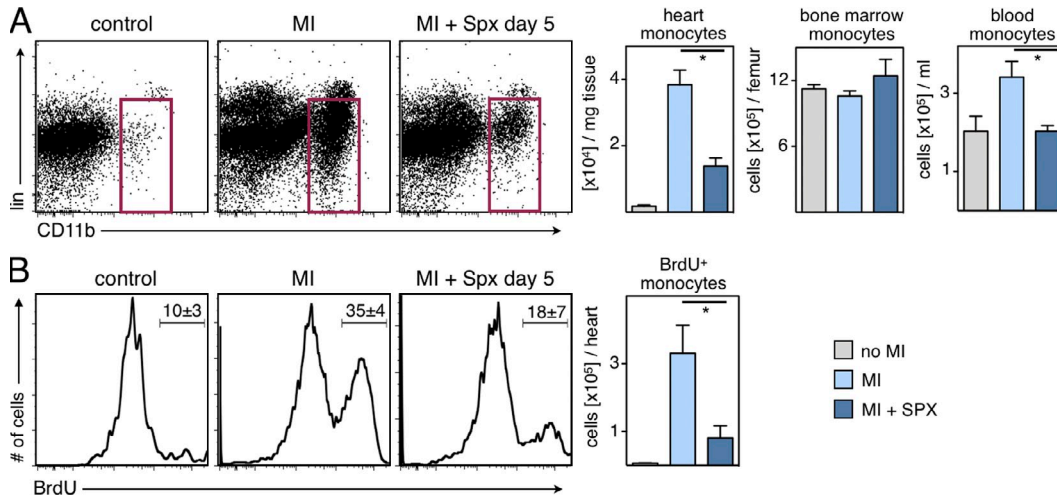


Figure 4. The spleen is a major source of Mo during acute inflammation. (A) Gate in dot plots of infarcted hearts shows myeloid cells on day 6 after MI (SPX indicates splenectomy 24 h before analysis; Lin indicates staining for lineage markers). Bar graphs enumerate total number of Mo in the heart, bone marrow, and blood ($n = 6-9$ per group, from three independent experiments). (B) Histograms gated on Mo in the heart. Bar graph shows the total number of BrdU⁺ Mo. Mean \pm SEM ($n = 4-6$ per group, experiment performed twice). *, $P < 0.05$.

The spleen is a major site of Mo production after MI

The reduction of BrdU⁺ Mo in infarct tissue 24 h after splenectomy could be explained by fast transfer of newly generated cells from the bone marrow to the spleen or by

splenic production of Mo. To test the latter hypothesis, we harvested splenocytes on day 6 after MI and assessed their colony-forming capacity. Using steady-state splenocytes from mice without MI as controls, we performed a

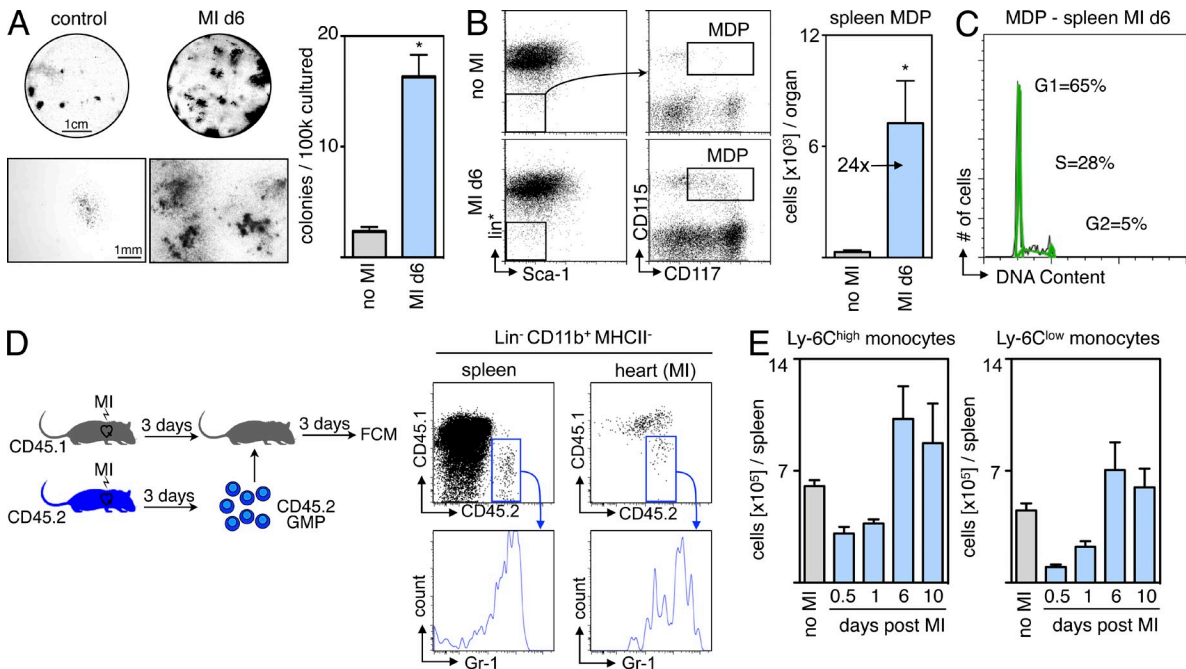


Figure 5. MI induces extramedullary monocytopoiesis in the spleen. (A) CFU assay of splenocytes from naive mice and from mice 6 d after MI ($n = 3$ per group, experiment performed twice). Top images show representative scans of the culture plate, bottom images show magnifications of colonies. (right) Bar graph enumerates colonies in cultures. (B) Representative dot plots from spleen and enumeration of splenic MDPs. lin* indicates lineage for myeloid progenitor staining as described in the Materials and methods section ($n = 6-9$ per group from three independent experiments). (C) Cell cycle analysis for splenic MDPs in mice after MI ($n = 3$ per group from one experiment). (D) Adoptive transfer of GMPs on day 3 after MI. CD45.2⁺ cells were transferred into infarcted CD45.1⁺ mice, which were analyzed 3 d later. Dot plots show adoptively transferred precursors in the splenic pool and the infarcted myocardium ($n = 6$ from one experiment). (E) Ly-6C^{high} and Ly-6C^{low} Mo in the spleen after MI. Mean \pm SEM ($n = 4-10$ per group from 4 independent experiments). *, $P < 0.05$.

CFU assay in medium with growth factors that promote myeloid colony formation, and found a sevenfold increase in CFU after MI (Fig. 5 A).

Encouraged by these data, we next defined the myelopoietic activity in the post-MI spleen more precisely. The most differentiated clonogenic precursor that can still give rise to Mo is the M Φ /dendritic cell precursor (MDP), which is defined by expression of CD115 (CSF1-R) and CD117 (c-kit) within the Lin^{low} IL-7R α ⁻ Sca-1⁻ population (Fogg et al., 2006; Auffray et al., 2009). FACS enumeration revealed a dramatic rise in splenic MDP numbers (Fig. 5 B), which started to increase 3 d after injury and peaked at 6 d after MI. The 24-fold increase in MDP was more pronounced than the increase in total myelopoietic activity, suggesting that splenic myelopoiesis after MI slants toward Mo production.

We then asked whether the splenic MDP population could give rise to their progeny in vivo. Cell cycle analysis using DAPI staining revealed that one third of the MDP population was in the S or G2 phase of the cell cycle (Fig. 5 C), indicating active proliferation. Fate mapping experiments involving adoptive transfer of granulocyte-M Φ progenitors (GMP, a population upstream of MDP in the development of Mo; Auffray et al., 2009) into mice with MI showed that the adoptively transferred precursors effectively contributed Mo to the splenic pool, which mobilized to the site of inflammation, the healing myocardium (Fig. 5 D). 3 d after

adoptive transfer of 10⁵ CD45.2⁺ myeloid progenitors, we found 27,306 \pm 2,841 transfer-derived Mo in the spleens and 16,850 \pm 2,080 in the infarcts of CD45.1⁺ recipient mice. Longitudinal assessment of Mo numbers in the spleen from day 1 to 10 after MI revealed a rapid refilling of the splenic Mo reservoir, which was replenished after 6 d (Fig. 5 E). Collectively, these findings suggest that splenic progenitor cells contribute importantly to the supply chain for Mo in acute inflammation and generate Mo that refill the splenic reservoir.

These newly described cell kinetics during acute inflammation are summarized in a model, in which we begin to describe the system-wide monocytic cell flux by addressing temporal and spatial aspects of the inflammatory response to injury (Fig. 6).

Serial in vivo imaging reveals a key function for the spleen in infarct healing

To explore the relevance of splenic monocytopoiesis for left ventricular remodeling and the evolution of heart failure, we designed a longitudinal imaging trial investigating the effects of spleen removal. Mice received permanent coronary artery ligation and were (a) followed up without further intervention, (b) splenectomized on the day of infarction, or (c) splenectomized 3 d after MI. On day 1 after MI, mice were evaluated by cardiac MRI. Initially, there were no significant differences between groups regarding either left ventricular ejection fraction or infarct size (Fig. 7).

In the same mice, we used noninvasive molecular imaging to map healing biomarkers related to MPS tissue functions. Phagocytic cells (CLIO-633), proteolysis (Prosense-750), and angiogenesis (IntegriSense-800) were quantified with multispectral fluorescence molecular tomography (FMT)-computed tomography (CT) after co-injection of three molecular imaging probes (Nahrendorf et al., 2009a). FMT-CT imaging on day 5 after MI showed that removal of the spleen resulted in reduced accumulation of CLIO-AF633, a nanoparticle targeted to Mo/M Φ (Nahrendorf et al., 2007a), in the infarct (Fig. 7). These data indicated reduced accumulation of phagocytic cells in the heart. Interestingly,

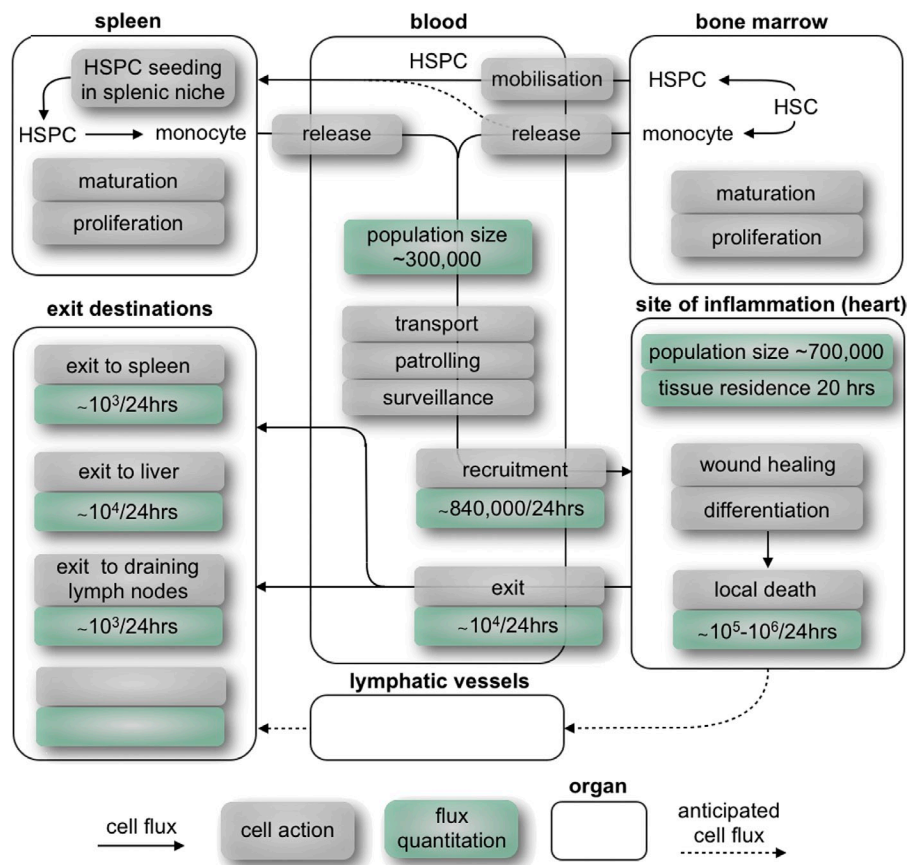


Figure 6. Current systemic MPS flux model in subacute MI in the mouse. The model was populated with numbers and rates obtained in mice with coronary ligation and is a first attempt at a more systematic visualization of system-wide cell kinetics in acute inflammation.

this reduced uptake was observed regardless of the timing of spleen removal. Prosense-750 activation also fell in splenectomized mice (Fig. 7), indicating lower proteolytic activity in infarcts (Nahrendorf et al., 2007a). The third imaging channel measured expression of the integrin $\alpha_v\beta_3$, a biomarker expressed by endothelial cells in neovessels and by fibroblasts (Nahrendorf et al., 2007a). The concentration of IntegriSense-800 in the infarct declined after splenectomy at either time point (Fig. 7).

Finally, we reimaged mice by cardiac MRI 3 wk after MI. We found that splenectomy at either time point significantly impaired left ventricular ejection fraction and resulted in a thinner scar, signifying infarct expansion and accelerated left ventricular remodeling (Fig. 7). Collectively, these data show that removal of the spleen reduced MPS-mediated healing biomarkers and accelerated the evolution of heart failure.

To relate the imaging findings to histological assessment of tissue healing, we evaluated additional cohorts of mice on day 7 after MI (Fig. 8). The removal of the spleen, either at the time of infarction or 3 d later, reduced the numbers of cells expressing CD11b and MAC-3. Neovascularization was impaired in mice that had been splenectomized, as indicated by a reduced number of CD31⁺ microvessels (Fig. 8). Three different methods were used

to analyze collagen deposition in the hearts after MI: Masson trichrome, picrosirius red staining, and immunoreactive staining for collagen I. All three showed reduced extracellular matrix and compromised healing of infarcts in mice without spleens (Fig. 8). As seen in the imaging trial, even late removal of the spleen, a site of monocytopoiesis, led to deteriorated wound healing.

Rapid Mo kinetics, local death, and splenic Mo production in stroke

To evaluate if our findings are applicable to other causes of acute inflammation, we examined Mo kinetics in mice with stroke. BrdU pulse-chase experiments revealed rapid Mo turnover kinetics in the brain after occlusion of the middle cerebral artery. On day 2 after stroke, 28 ± 6% of all CD11b⁺ lineage⁻ cells in the brain were BrdU⁺ after receiving BrdU pulses 12 and 24 h before tissue harvest (Fig. 9 A). This CD11b⁺ lineage⁻ population includes resident microglia (Graeber, 2010), whereas inflammatory Ly-6C^{high} Mo are not found in brain tissue of healthy mice. Specifically, CD11b⁺ microglia are Ly-6C^{low} (Duncan and Miller, 2011). Analyzing the turnover of inflammatory Ly-6C^{high} Mo in the ischemic brain, we found comparable numbers to those seen in myocardial infarcts: 44 ± 9% of Ly-6C^{high} Mo were BrdU⁺ 24 h after BrdU pulses (Fig. 9 B). These data imply that

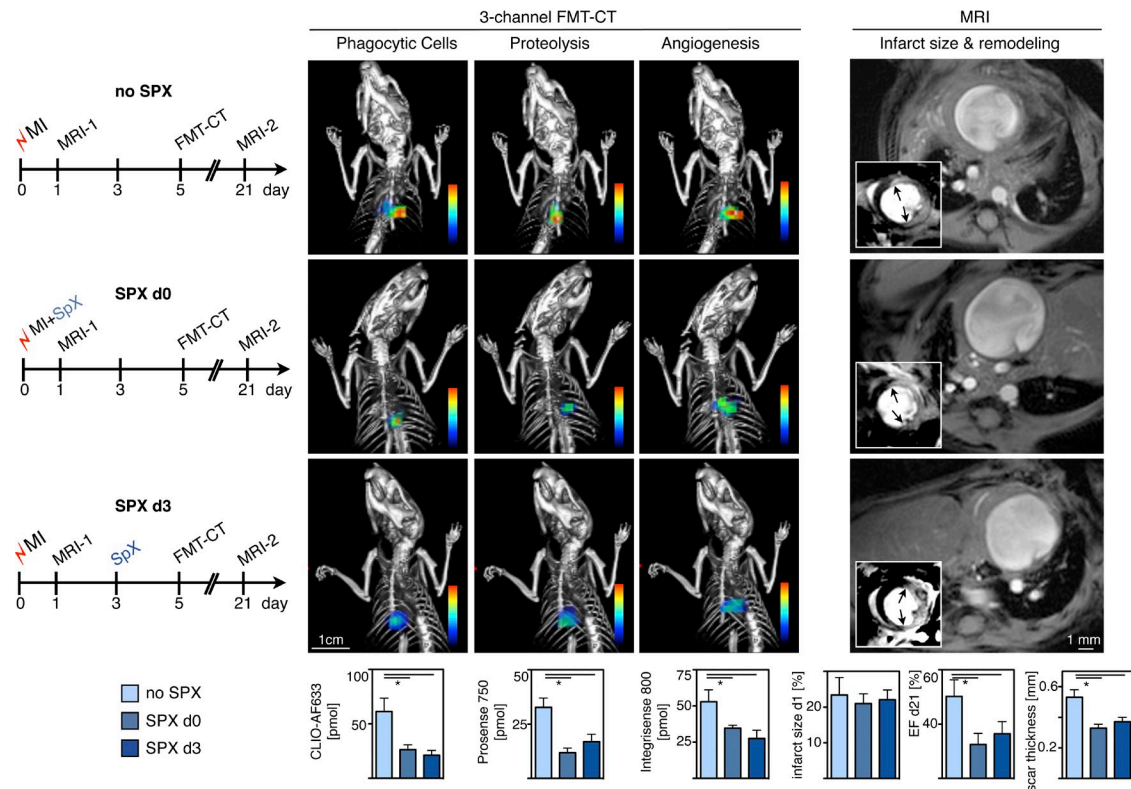


Figure 7. Serial in vivo imaging reveals key function of splenic Mo/MΦ in infarct healing. Study groups: MI and no SPX (top row), MI and SPX on d0 (middle), and MI and SPX on d3 after MI (bottom). Three-channel FMT-CT was done on day 5 after MI. Bar graphs on the bottom show fluorescence signal in the infarct in respective channels. MR images from day 1 (inset) and day 21 (full size) are shown on the right, with bar graphs on the bottom. Arrows indicate gadolinium-DTPA enhanced infarct. Mean ± SEM (n = 8–12 per group from two experiments). *, P < 0.05.

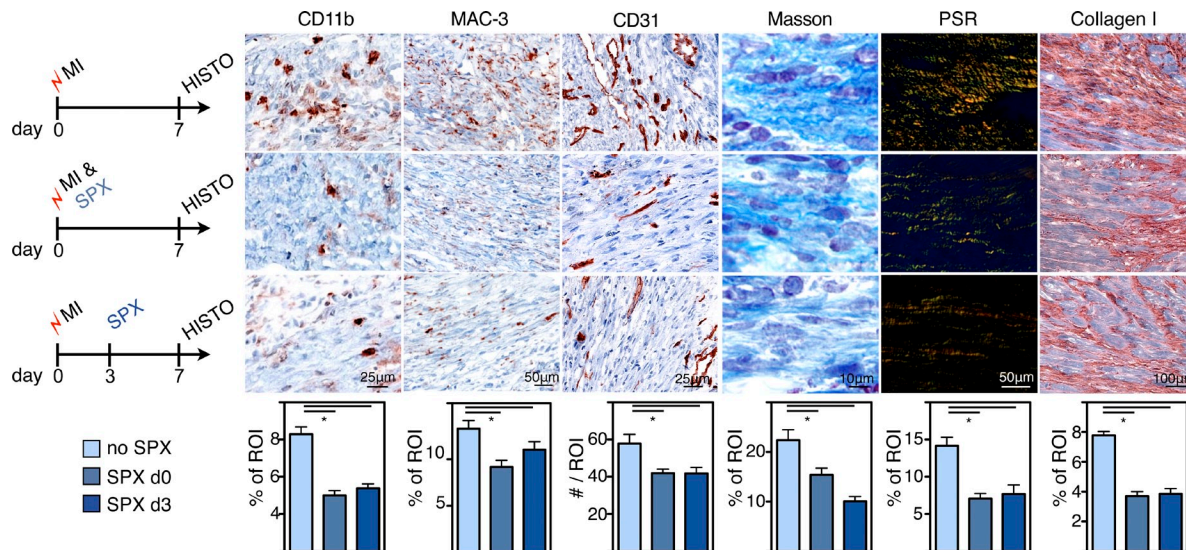


Figure 8. Histological biomarkers of infarct healing after splenectomy. Experimental groups: MI and no SPX (top row), MI and SPX on d0 (middle), and MI and SPX on d3 after MI (bottom). IHC staining for myeloid cells (CD11b), MΦ (MAC-3), neo-vascularization (CD31), and collagen deposition (Masson trichrome, picrosirius red [PSR], and collagen I). ROI, region of interest. Mean \pm SEM ($n = 5$ per group from one experiment). *, $P < 0.05$.

Mo flux rates are not only high in MI but also in other acutely ischemic tissues.

Next, we assessed local death rates of Mo in ischemic brain tissue. We found that $2 \pm 0.2\%$ of Mo were caspase-3⁺ on day 2 after induction of stroke. On day 4, the percentage of Mo undergoing apoptosis was $6 \pm 0.5\%$, comparable to the data in MI.

We also enumerated Mo in the spleen in mice with stroke. Their number was reduced by 48% on day 2 after injury ($P = 0.03$; Fig. 9 C), indicating that the splenic Mo reservoir supplied the injured brain tissue. Finally, we assessed splenic monocytopoiesis 10 d after stroke by enumeration of MDPs. We found that numbers of splenic MDPs increased eightfold ($P < 0.01$; Fig. 9 D) and concluded that the spleen is a site of Mo production after stroke, comparable to the situation after MI.

IL-1 β signaling and splenic monocytopoiesis

To identify pathways involved in extramedullary monocytopoiesis after MI, we screened spleen mRNA levels after MI for a variety of candidate cytokines and growth factors, including IL-1 α , IL-1 β , TNF, IL-6, CXCL12, VCAM-1, ICAM, M-CSF, GM-CSF, and G-CSF. Interestingly, we only found a marked sustained increase in the expression of IL-1 β (Fig. 10 A and not depicted). An ELISA confirmed a significant increase of IL-1 β protein in the spleen on day 6 after MI (Fig. 10 A).

We next induced MI in mice lacking the IL-1 receptor (IL-1R^{-/-}) and assessed splenic monocytopoiesis 6 d thereafter. The number of CFUs was markedly reduced in IL-1R^{-/-} spleens (Fig. 10 B), and MDPs were reduced by 67% in IL-1R^{-/-} mice when compared with WT (2.3×10^3 vs. 6.1×10^3 ; $P = 0.005$; Fig. 10 C). In addition, the number of newly made BrdU⁺ Mo was reduced from 2.9×10^4 in WT mice to

1×10^4 in IL-1R^{-/-} ($P = 0.001$; Fig. 10 C). Although infarcts from WT mice contained 3.7×10^4 Mo per mg tissue, infarcted hearts from IL-1R^{-/-} recruited only 2.0×10^4 Mo ($P = 0.01$; Fig. 10 C). This decrease paralleled our estimation of what the spleen contributes to the Mo population in the infarct (Fig. 4).

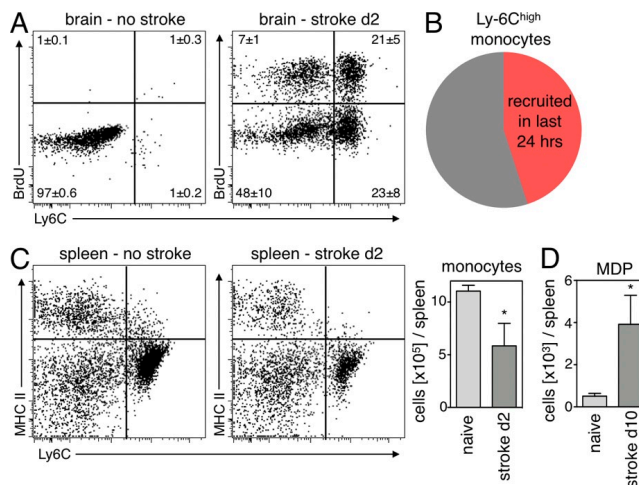


Figure 9. Rapid Mo kinetics and supply of splenic Mo in stroke.

(A) Dot plots from brain tissue gated on CD11b⁺ and lineage⁻ cells 24 h after BrdU pulse. Mean \pm SEM ($n = 4-5$ per group; $P < 0.05$ stroke vs. no stroke). (B) Pie chart illustrates turnover of Ly-6C^{high} Mo in the brain on day 2 after stroke. (C) Number of Mo in the spleen after stroke. Dot plots are gated on CD11b⁺ lin⁻ cells and compare naive control mice to mice 2 d after stroke. Bar graph shows total Mo in the spleen. Mean \pm SEM (*, $P < 0.05$; $n = 4-5$ per group from one experiment). (D) Increased MDP on day 10 after stroke in the spleen. Mean \pm SEM (*, $P < 0.05$, $n = 4-5$ per group from one experiment).

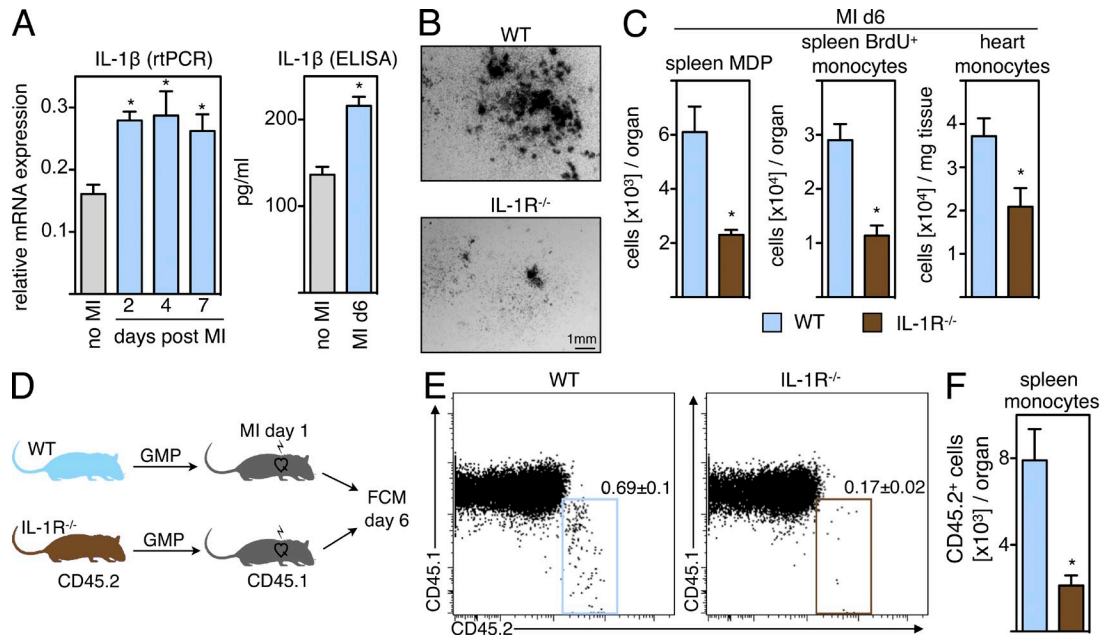


Figure 10. IL-1 β is a key cytokine for splenic monocytopoiesis. (A) rtPCR of IL-1 β mRNA expression in the spleen throughout the first week after MI ($n = 6-7$ per group; *, $P < 0.05$). IL-1 β protein by ELISA in the spleen on day 6 after MI ($n = 4$ per group; *, $P < 0.05$). (B) Cultured spleen cells from WT and IL-1R^{-/-} mice colony forming capacity on day 6 after MI. Experiment was done in duplicates. (C) Enumeration after FCM analysis on day 6 after MI of splenic MDPs (left), BrdU⁺ Mo in the spleen (middle), and in the heart (right) of IL-1R^{-/-} mice compared with WT. Mean \pm SEM ($n = 5$ per group; *, $P < 0.05$). (D) Setup of the experiment: Adoptive transfer of CD45.2⁺ GMPs into infarcted CD45.1⁺ mice 1 d after MI. Analysis was performed 5 d later, comparing the capacity of transferred cells to generate Mo in the presence (WT) or absence (IL-1^{-/-}) of the IL-1R. (E) Dot plots from spleens are gated on Mo, identified as CD11b⁺, lineage⁻, and CD11c⁻. Mean percentage \pm SEM ($n = 4$ recipients per group). (F) Enumeration of CD45.2⁺ Mo in the spleens of CD45.1⁺ recipients 6 d after MI and 5 d after adoptive transfer. Mean \pm SEM ($n = 4$ per group; *, $P < 0.05$).

To investigate if the reduction of splenic monocytopoiesis is caused by the absence of the IL-1R on myeloid progenitors, we adoptively transferred FACS-sorted GMPs from either WT or IL-1R^{-/-} mice (both CD45.2⁺) into CD45.1⁺ mice, 1 d after MI (outlined in Fig. 10 D). Flow cytometric analysis 5 d later revealed that even though each recipient had received the same number of progenitor cells (10⁵), CD45.2⁺ progeny was significantly reduced in mice that were injected with IL-1R^{-/-} GMPs (2,123 \pm 463 Mo after transfer of IL-1R^{-/-} GMPs vs. 7,907 \pm 1,436 WT; $P = 0.008$; Fig. 10, E and F). These results indicate that direct IL-1 signaling on myeloid progenitors controls splenic monocytopoiesis.

DISCUSSION

Our knowledge of innate immune cell function has rapidly expanded in the last decade, but cell kinetics, especially turnover rates in inflamed tissue, remain incompletely understood. Conventional wisdom suggested that a large population of Mo is recruited at initiation of acute inflammation, that these cells pursue their specific function for the duration of the acute inflammatory process, and that their presence wanes when inflammation resolves. This study used an acute inflammatory state in the heart to fate map Mo/M Φ and to determine their turnover rates in tissue. Contrary to preconception, we found extremely rapid kinetics. Mo spent a mean of 20 h at the site of inflammation, and within 24 h the majority of

the population was replaced by a new generation of cells, even days after initiation of inflammation. Collectively, these findings allow one to construct simple models of in vivo cell kinetics (Fig. 6).

The spleen furnished most of this constant stream of Mo. Recent work found that the spleen contains a readily mobilizable emergency reservoir of Mo that exhausts in the first hours after injury (Swirski et al., 2009). We now report that the spleen provides cells continuously to satisfy the persistently high demand at the site of inflammation. Surgical removal of the spleen several days after coronary ligation substantially reduced the number of Mo recruited to the infarct and led to impaired wound healing and heart failure. Interestingly, we found a robust expansion of myeloid progenitor cells (MDP) in the spleen, indicating that the organ hosted niches for extramedullary emergency monocytopoiesis. Adoptive transfer of upstream progenitors (GMP) resulted in splenic seeding, and the transferred cells gave rise to splenic Mo, which then traveled to the site of inflammation. (We do not yet know how many of these Mo differentiate into M Φ once they have entered the infarct; we did not pursue this question because of the technical limitations of fate mapping methods, i.e., Mo activation and initiation of differentiation during cell sorting for adoptive transfer.) The initial loss of splenic Mo during the onset of injury, when the spleen's reservoir departs, recovers quickly, as the cell numbers in the spleen reached preinjury

levels in <1 wk. Mice with stroke experienced a similar departure of splenic Mo followed by increased progenitor activity. Collectively, these data position the spleen as a major site of inflammatory Mo production in acute inflammation.

We identified IL-1 β as a signal for splenic Mo production after MI, in line with previous insight on the cytokine's role in the expansion of progenitors (Brugger et al., 1993; McKinstry et al., 1997). In parallel to our findings in the spleen, IL-1 β also appears to regulate prenatal extramedullary hematopoiesis in the liver (Orelia et al., 2009). The cytokine's expression increases in patients and rodents after MI (Balbay et al., 2001; Li et al., 2006). Thus, although regulation of hematopoiesis relies on multifactorial mechanisms (Brugger et al., 1993), these data point toward a key role for IL-1 β in triggering extramedullary monocytopoiesis after MI.

After the initial surge of Mo/M Φ in the infarct, the overall size of the cell population at the inflammatory site remained stable for several days, despite ongoing large-scale recruitment. Hence, we investigated what mechanism accounts for clearance of cells from the infarct. We found that the high recruitment rates were matched by rapid cell death. Frequency and duration of apoptotic events suggested that death could clear as many cells from the infarct as were newly recruited. Interestingly, we found that the frequency of apoptotic Mo/M Φ increased at later time points, from <2% on day 3 to >4% on day 6 after MI. At the same time, cell recruitment decelerated from 43% BrdU⁺ cells on day 3 versus 35% on day 5. These results indicate that the balance of cell recruitment and local cell death regulated the overall size of the Mo/M Φ population. Death rates were higher and recruitment slower at later time points; therefore, when apoptotic death exceeds recruitment, the cell population contracts and resolution of inflammation commences.

Intriguingly, we observed cell exit using organ transplantation and two independent methods of egress detection: radioactively labeled nanoparticles and flow cytometric staining for CD45.1/2 leukocyte surface markers. Both methods indicated that between 5 and 13% of the cell population departed from the site of inflammation within 24 h, a pathway of cell clearance outweighed by cell death. With both techniques, we found \sim 10,000 exited cells in circulating blood. Liver, spleen, and lymph nodes were the dominant destination organs. Not surprisingly, the numbers of cells detected in these scavenging organs were somewhat higher when we used a nonbiodegradable label. The CD45.1/2 leukocyte surface marker approach has previously revealed cell exit from transplanted, regressing atherosclerotic vascular beds in a setting of resolving chronic inflammation. These studies implied that certain lipids may inhibit cell migration (Llodrá et al., 2004). Future work must determine the biological relevance of cell exit beyond mere reduction of cell numbers in the inflammatory site. These observations might reflect a passive "spill over" phenomenon without consequence. Alternatively, cell exit may be an active process that enables exchange of information through cell-cell contacts and entertains long-distance feedback loops.

These new insights into the life cycle of Mo/M Φ can guide identification of novel therapeutic strategies. Because the tissue residence time of Mo in acute inflammation is as short as 20 h in the mouse, and because continuous cell recruitment occurs on a large scale, therapies that target cell production, for instance in the splenic niche, may produce favorable outcomes. Mo recruitment appears to be an attractive target beyond the first hours of injury. Manipulating the recruitment/death balance could induce resolution if inflammation lingers and threatens to compromise tissue repair. Notably, the reported cell kinetics apply to acute inflammation; further investigations should probe how chronic inflammatory processes differ.

The data were collected in a type of tissue injury with high clinical relevance. Many patients with myocardial ischemia likely suffer from exuberant or prolonged inflammation, which may exacerbate injury or hinder swift repair (Maekawa et al., 2002; Nahrendorf et al., 2010b). Exaggerated infarct inflammation, a situation previously modeled in mice with atherosclerosis (Leuschner et al., 2010; Panizzi et al., 2010) and frequently found in patients with atherosclerotic disease, impedes efficient infarct healing and promotes left ventricular dilation (Nahrendorf et al., 2010b). The current serial imaging data in WT mice with coronary ligation underline the role of the spleen in recovery after MI, with the limitation that splenectomy neutralizes a variety of immune cells that might affect the remodeling differently. In patients with acute MI, high Mo blood levels correlate inversely with ejection fraction (Tsujioka et al., 2009), which is a strong predictor of mortality. Therefore, insight into infarct cell kinetics and the fate of Mo/M Φ in MI provide a much needed foundation for developing novel therapy options in heart failure, a condition that afflicts 5 million patients in the United States and carries an annual mortality of up to 50% (Roger et al., 2011).

MATERIALS AND METHODS

Mouse models. MI was induced by permanent coronary ligation as described previously (Leuschner et al., 2010). In brief, mice were anesthetized with Isoflurane (2%/2 liters O₂), intubated, and ventilated with an Inspira Advanced Safety Single Animal Pressure/Volume Controlled Ventilator (Harvard Apparatus). The chest wall was shaved, and left thoracotomy was performed in the fourth left intercostal space. The left ventricle was visualized, and the left coronary artery was permanently ligated with monofilament nylon 8-0 sutures (Ethicon) at the site of its emergence from under the left atrium. The chest wall was closed with 7-0 nylon sutures and the skin was sealed with superglue.

Splenectomy was performed using Isoflurane anesthesia. The mouse's abdominal cavity was opened, the spleen vessels were cauterized, and the spleen was carefully removed (Swirski et al., 2009).

Hearts were transplanted into the recipients' peritoneal cavity by establishing an end-to-side anastomosis of the donor aorta to the recipient aorta and an end-to-side anastomosis of the donor pulmonary trunk to the inferior vena cava, as described previously (Swirski et al., 2010). The total operative time was in the range of 30–40 min. The ischemia time for the transplanted heart was 15.1 ± 0.9 min. If myocardial contractions were not palpated through the abdomen, the procedure was considered a surgical failure and the mouse was excluded from experiments. To create the same systemic immune environment, we infarcted both graft donors and recipients.

For stroke induction, we used the middle cerebral artery occlusion model (Qiu et al., 2008). Animals were anesthetized with Isoflurane (2%/2 liters O₂). A silicone-coated 8–0 monofilament (Doccol Corporation) was introduced in the internal carotid artery and advanced to occlude the middle cerebral artery for 45 min. Regional cerebral blood flow was measured by laser-Doppler (ML191; AD Instruments Inc.) using a flexible probe, placed over the temporal bone after removal of part of the temporalis muscle, to confirm occlusion and reperfusion. Rectal temperature was maintained between 36.5°C and 37.5°C with a homeothermic blanket (Frederick Haer and Co.).

Female C57BL/6J (CD45.2⁺), B6.SJL-Ptprca Pepcb/BoyJ (CD45.1⁺) and B6.129S7-Il1r1^{tm1lmx}/J (IL-1R^{-/-}) mice were purchased from The Jackson Laboratory. All animal experiments were approved by Massachusetts General Hospital's Institutional Review Committee.

Flow cytometry. To prepare single-cell suspensions from infarct tissue, hearts were harvested; minced with fine scissors; placed into a cocktail of collagenase I, collagenase XI, DNase I, and hyaluronidase (Sigma-Aldrich); and shaken at 37°C for 1 h. Cells were then triturated through nylon mesh and centrifuged (15 min, 500 g, 4°C).

Brain hemispheres were removed, triturated in HBSS with 15 mM Hepes and 0.5% glucose, and homogenized. Cells were then separated using a 70–30% Percoll solution.

Spleens were removed, triturated in HBSS (Mediatech, Inc.) at 4°C with the end of a 3-ml syringe, and filtered through nylon mesh (BD). The cell suspension was centrifuged at 300 g for 8 min at 4°C. Red blood cells were lysed with ACK lysis buffer, and the splenocytes were washed with HBSS and resuspended in HBSS supplemented with 0.2% (wt/vol) BSA and 1% (wt/vol) flow cytometry. Peripheral blood was drawn via cardiac puncture with citrate solution (100 mM Na-citrate, 130 mM glucose, pH 6.5) as anticoagulant, and red blood cells were lysed with ACK lysis buffer. Additionally, single-cell suspensions were obtained from liver and skeletal muscle by digestion with the cocktail described above. Single-cell suspension from lymph nodes was obtained by trituration in HBSS and filtering through nylon mesh.

Total viable cell numbers were determined from aliquots using a hemacytometer with Trypan blue (Mediatech, Inc.).

Cell suspensions were incubated in a cocktail of mAbs against T cells (CD90-PE), B cells (B220-PE), NK cells (CD49b-PE and NK1.1-PE), erythroid cells (Ter-119-PE), granulocytes (Ly-6G-PE), myeloid cells (CD11b-PE), dendritic cells (CD11c-PE), Mo subsets (Ly-6C-FITC), MΦ (F4/80-PE-Cy7), antigen-presenting cells (I-Ab-APC), CD45.2-expressing cells (CD45.2-PerCP), CD45.1-expressing cells (CD45.1-APC), cells expressing IL-7 receptor α chain (IL-7RA-PE), c-kit⁺ cells (CD117-PE-Cy7), against Fcγ III/II receptor (CD16/CD32-APC-Cy7), Sca-1 (CD34-Alexa Flour 700), hematopoietic progenitor cells (CD34-FITC), and monoblasts (CD115-APC; all antibodies from BD or BioLegend). Cell cycle analysis was performed using FxCycle violet stain (Invitrogen). Caspase-3-FITC (active form; BD) was used for staining of apoptotic cells. Mo/MΦ were identified as CD11b^{high} (CD90/B220/CD49b/NK1.1/Ly-6G)^{low} Ly-6C^{high/low}. Mo were identified as CD11b^{high} (CD90/B220/CD49b/NK1.1/Ly-6G)^{low} (F4/80/CD11c)^{lo} Ly-6C^{high/low}. MΦ/dendritic cells were identified as CD11b^{high} (CD90/B220/CD49b/NK1.1/Ly-6G)^{low} (F4/80/CD11c)^{high} Ly-6C^{low}. Neutrophils were identified as CD11b^{high} (CD90/B220/CD49b/NK1.1/Ly-6G)^{high} (F4/80/CD11c)^{low} Ly-6C^{int}. Reported cell numbers were calculated as the product of total living cells (total viable leukocytes per ml) and percentage of cells within the Mo/MΦ gate. Within this population, Mo subsets were identified as (F4/80/I-A^b/CD11c)^{low} and either Ly-6C^{high} or Ly-6C^{low}. Cell numbers were normalized for the weight of the infarct in milligrams, yielding the number of Mo per mg tissue. For transplant experiments, cells were identified as described above and then plotted comparing CD45.2 vs. CD45.1. Within the (CD90/B220/CD49b/NK1.1/Ly-6G/CD11b/CD11c)^{low} IL-7Rα⁻ Sca-1⁻ population, MDPs were defined as CD117^{int} CD115⁺, whereas GMPs were identified as CD117⁺ CD34⁺ CD16/32⁺. Data were acquired on an LSR II (BD) and analyzed with FlowJo

v.8.5.2 (Tree Star, Inc.). For the detection of CLIO-VT750 (24 h after the injection of 15 mg of Fe/kg bodyweight), a filter configuration of 755/LP and 780/60 was used.

Analysis of proliferation with BrdU. For proliferation studies two time-points were chosen for analysis: day 3 and 5 after MI. For stroke experiments, we analyzed tissues on day 2 after injury. Mice were injected i.p. with 1 mg BrdU (BD; Dolbeare et al., 1983) 12 and 24 h before analysis to allow incorporation into dividing cells. After tissue harvest, cells were processed and stained with anti-BrdU-APC against T cells (CD90-PE), B cells (B220-PE), NK cells (CD49b-PE and NK1.1-PE), granulocytes (Ly-6G-PE), red blood cells (Ter-119-PE), myeloid cells (CD11b-APC-Cy7), DCs (CD11c-Alexa Flour 700), MΦ (F4/80-PE-Cy7), and Mo subsets (Ly-6C-FITC) according to the manufacturer's protocol (BD).

Measurement of Mo/MΦ exit by heart transplantation and flow cytometry. To investigate whether Mo leave the site of inflammation and, if so, in what amounts, we infarcted C57BL/6J (CD45.2⁺) and B6.SJL-Ptprca Pepcb/BoyJ (CD45.1⁺) mice and transplanted the infarcted hearts from CD45.2⁺ into CD45.1⁺ mice 3 d later. MI was induced in both donor and recipient to generate the same systemic immune environment of post-MI healing. 24 h after transplantation, mice were sacrificed, and their organs were harvested and processed for flow cytometric analysis as described above. Allelic labeling allowed the detection of donor-derived Mo that had departed the transplanted organ, identified as CD11b^{high} (CD90/B220/CD49b/NK1.1/Ly-6G)^{low} (F4/80/CD11c)^{low} Ly-6C^{high/low} and CD45.2^{high}. We normalized the cumulative number of retrieved donor-derived Mo in the recipient to the number of Mo found in the infarcted heart to calculate the percentage of exited Mo.

Adoptive transfers. MI was induced in CD45.1⁺ mice. For analysis of distribution and differentiation, 3 d later the mice were injected i.v. with 10⁵ GMP obtained by fluorescence-activated cell sorting (on FACSaria; BD) from the bone marrow of CD45.2⁺ mice that had undergone infarct surgery at the same time point as cell recipients. For comparison of WT versus IL-1R^{-/-} GMP transfer, cells were injected 1 d after MI. The multicolor antibody staining for GMP described above was also used for cell sorting, resulting in cell population purity of >99.5%. 3 (experiment described in Fig. 5 D) or 5 d (Fig. 10 D) after intravenous injection of CD45.2⁺ GMP, recipients were sacrificed and the transferred cells were fate-mapped by flow cytometric analysis.

Measurement of cell exit using a Mo/MΦ-targeted nanoparticle. One limitation of measuring cell exit by flow cytometric detection of the donor leukocyte antigen CD45.2 in the graft recipient's potential target organs is that the antigen might be scavenged rapidly, which renders it undetectable. We therefore devised a labeling strategy using a nonbiodegradable, radioactive tag on iron-oxide nanoparticles (¹¹¹In-CLIO) that target Mo/MΦ (Nahrendorf et al., 2008). ¹¹¹InCl₃ (3.01 mCi, 114.7 MBq) was diluted with 20 μl ammonium acetate (0.4 M, pH 5.5) and added to CLIO-DTPA (250 μg) dissolved in 40 μl ammonium acetate (0.4 M, pH 5.5) and incubated for 30 min at 75°C. After cooling to room temperature, the mixture was purified using a PD-10 column. Fractions containing ¹¹¹In-CLIO-DTPA were concentrated using microcentrifuge filters (MWCO = 50 kD). Concentrated ¹¹¹In-CLIO-DTPA (2.71 mCi, 100.3 MBq; 87.4% RCY) was diluted with 1xPBS to a volume of 100 μl for injection. MI was induced in two mice. On day 2 after MI, mice were injected with 1.1 ± 0.1 mCi ¹¹¹In-CLIO-DTPA. On day 3 after MI and 24 h after injection of the nanoparticle, hearts were explanted and their activity was measured by γ counting (1480 Wizard 3[™]; PerkinElmer) while they were immersed in chilled buffer. After scintillation counting, hearts were immediately transplanted as described above. Recipient mice were dissected 24 h later, and their organs were measured by γ counting. Organ activity measurements were decay-corrected to the time of transplantation. The decline in radioactivity of the grafted heart after 24 h residence in an uninjected recipient mouse reflected

the nanoparticle's departure from the organ and, because this nanoparticle distributes to Mo/MΦ, by extension also the departure of these cells. The decay-corrected activity of explanted hearts was divided by the average number of Mo present in the infarct, which yielded radioactivity per Mo. This number was then used to calculate the Mo cell content per organ in the transplant recipient by multiplying the photon counts measured in the respective organ with the activity per Mo.

Live cell imaging of Mo death. Splenic Mo were enriched by lineage depletion using MACS LD columns (Miltenyi Biotec) and PE-conjugated antibodies against B220, CD49b, NK1.1, Ly-6G, CD90, and Ter-119, followed by anti-PE magnetic beads (Miltenyi Biotec). The cells were then incubated with Annexin V-FITC (BD) antibodies and PI (BD). Imaging began after 30 min of incubation to allow primary antibody binding. The sample was prepared on a slide with coverslip and imaged at 37°C with an Olympus IX71 inverted fluorescence microscope customized with an X-Y-Z motion controller with stage assembly (Applied Precision) and a Photometrics HQ2 CCD camera (Photometrics). 10 field of views, each with 1–4 cells present, were imaged for 2 h, with 5-min intervals. Signal was plotted as a function of time, and the delay between onset of Annexin-V signal (early stage apoptosis) to PI (complete cell death) was analyzed in MATLAB (The Mathworks).

Tissue colony forming cell assay. To determine the number of myeloid colony-forming units in the spleen in the steady-state and after MI, a single-cell suspension was prepared from the spleens of naive mice and those that had received coronary ligation 6 d before analysis. 3×10^5 splenocytes were plated in triplicates in complete methyl cellulose medium (MethoCult GF M3434; StemCell Technologies) according to the manufacturer's instructions. Counts were performed after 10 d of culture in a humidified incubator at 37°C, 5% CO₂. At least three independent samples per group were analyzed. Counts were normalized to the number of cells initially plated.

FMT-CT. For serial in vivo imaging, three groups of mice were investigated: mice with MI (MI, no Spx), mice with MI and splenectomy on the same day (MI+Spx d0), and mice with MI and splenectomy on day 3 after MI (MI+Spx d3; $n = 8-12$ per group). On day 5 after MI, we performed FMT-CT imaging (Nahrendorf et al., 2009b; Panizzi et al., 2010) to interrogate the magnitude of inflammation. Using three-channel acquisition allowed simultaneous analysis of phagocytic activity (CLIO-VT680), proteolytic activity (Prosense-750; PerkinElmer) and angiogenesis (Integrisense-800). Data were acquired 24 h after injection of 15 mg/kg of CLIO-VT680, 5 nmol of the pan-cathepsin protease sensor Prosense-750 and 5 nmol of the integrin binding sensor Integrisense-800. A 3D FMT dataset was reconstructed in which fluorescence per voxel was expressed in nM. To robustly identify the region of interest in the heart, anatomical imaging with CT preceded FMT. The imaging cartridge containing the anesthetized mouse was placed into the Plexiglas holder that supplied Isoflurane, warm air, and optimal positioning in the CT (Inveon PET-CT; Siemens). The CT x-ray source operated at 80 kVp and 500 μA with an exposure time of 420 ms. The effective 3D resolution was 80 μm isotropic. Isovue-370 was infused intravenously at 40 μl/min through a tail vein catheter. The CT reconstruction protocol performed bilinear interpolation, used a Shepp-Logan filter and scaled pixels to Hounsfield units.

Image fusion of FMT with CT realized three-dimensional mapping of fluorescence within the anatomical reference CT. The approach was based on a multimodality-compatible animal holding device that provides fiducial landmarks on its frame (Nahrendorf et al., 2010a). The imaging cartridge lightly compressed the anesthetized mouse between optically translucent windows and thereby prevented motion during transfer between modalities. The three-dimensional distribution of the fiducials enabled automated co-registration of datasets. The point based co-registration tool kit in OsiriX shareware (64 bit, version 3.5.1) fused images after identification of fiducials in respective modalities. Fiducials were tagged with point markers to define their XYZ coordinates. Using these coordinates, data were resampled,

rotated, translated to match the image matrices, and finally fused. Fusion was done on a Macintosh computer with a quad-core processor, 16GB RAM, and an NVIDIA GeForce graphic card.

MRI. We performed in vivo MRI on days 1 and 21 after MI in mice with splenectomy on the day of MI, splenectomy 3 d after MI and without splenectomy ($n = 8-12$ per group). A 7 Tesla horizontal bore Pharmascan (Bruker) and a custom-made mouse cardiac coil in birdcage design (Rapid Biomedical) were used to obtain cine images of the left ventricular short axis. We used ECG and respiratory gating using a gradient echo sequence (echo time 2.7 ms, 16 frames per RR interval; flip angle 30 degrees [or 60 degrees for delayed enhancement imaging]; in-plane resolution 200×200 μm; slice thickness 1 mm). The infarcted area was identified in end-diastolic frames as: (a) hypokinetic in cine-loops and (b) hyperenhancing after injection of gadolinium-diethylenetriaminepentaacetic acid (Berlex) at a dosage of 0.3 mmol/kg. Cardiac volumes and infarct size were quantitated from 6–8 short axis imaging slices covering the left ventricle, as described previously (Leuschner et al., 2010; Panizzi et al., 2010).

Histology. Histology of hearts was assessed on days 3 and 6 after MI for immunofluorescence double staining with the TUNEL and CD11b. Hearts were excised, rinsed in PBS, and flash-frozen in O.C.T. compound (Sakura Finetek) with isopentane on dry ice. Fresh-frozen serial 5-μm thick sections were stained with the TUNEL reagents (DeadEnd Fluorometric TUNEL System, Promega) according to the manufacturer's protocol, and then incubated with a rat anti-mouse CD11b antibody (M1/70; BD), followed by a biotinylated secondary antibody. Streptavidin-Texas red (GE Healthcare) was used to detect the CD11b antibody, and the slides were coverslipped using a mounting medium with DAPI (Vector Laboratories) to identify cell nuclei. Images were captured and processed using an epifluorescence microscope, Nikon Eclipse 80i (Nikon Instruments Inc.), with a Cascade Model 512B camera (Roper Scientific).

For immunohistochemistry, heart histology was assessed on day 7 after MI. The tissue sections were stained for Mo (CD11b: M1/70; BD), MΦ (MAC-3; BD), neovessels (CD31: PECAM-1; BD), and collagen deposition (Collagen I; Abcam). The appropriate biotinylated secondary antibodies, ABC kit (Vector Laboratories, Inc.) and AEC substrate (Dako) were used for color development, and all the sections were counterstained with Harris hematoxylin. For collagen analysis, Trichrome stains (MASSON; Sigma Aldrich) and picrosirius red stains (Polysciences, Inc.) were performed according to the manufacturers' protocols, and the picrosirius red stained sections were analyzed using Nikon 50i (Nikon) equipped with a D-PP DIC rotatable polarizer (NBN74940). The positive area or cell numbers were quantified using IPLab (version 3.9.3; Scanalytics, Inc.) and analyzing five high power fields per section and per animal at magnification 200× or 400×.

Quantitative PCR. Total mRNA from heart tissue was isolated by QIAGEN RNeasy Mini kit. Oligo(dT)-based cDNA was generated by use of the SuperScript III First-Strand Synthesis kit (Invitrogen), which made cDNA only from the mRNA portion of the total RNA pool. Multiplex quantitative PCR was performed on triplicate samples using Applied Biosystems TaqMan Assays. Infarct tissue was examined for expression of IL-1α, IL-1β, TNF, IL-6, CXCL12, VCAM-1, ICAM, M-CSF, GM-CSF, G-CSF, and appropriate controls (GAPDH). Gene expression was determined as x-fold difference after normalizing to GAPDH loading control.

Cytokine assay. Blood was drawn via cardiac puncture at the time of euthanasia and allowed to clot at 37°C for 20 min. Serum was collected by centrifuging at 10,000 g for 5 min. Spleens were removed, homogenized, and centrifuged at 300 g for 8 min. Supernatants and serum samples were stored at -80°C until time of analysis. A mouse-specific ELISA kit (Quantikine) for IL-1β was obtained from R&D Systems, and samples were processed according to the manufacturer's instructions.

Statistics. Results are expressed as mean ± SEM. Statistical comparisons between two groups were evaluated by Student's *t* test and corrected by ANOVA for multiple comparisons. A value of $P < 0.05$ was considered to indicate statistical significance.

Online supplemental material. The supplemental discussion contains modeling of the infarct-resident cell population on day 3 after MI. Online supplemental material is available at <http://www.jem.org/cgi/content/full/jem.20111009/DC1>.

We gratefully acknowledge the help of Michael Waring and Adam Chicoine (Ragon Institute Flow Core Facility), Dr. Colvin (MGH Pathology), and Joshua Dunham (CSB Mouse Imaging Program).

This work was funded in part by grants from the National Heart, Lung, and Blood Institute (R01HL095629 and R01HL096576) and the American Heart Association (SDG0835623D) to M. Nahrendorf; R24-CA92782 and Translational Program of Excellence in Nanotechnology U01-HL080731/HHSN268201000044C to R. Weissleder; Deutsche Herzstiftung e. V. to F. Leuschner; Boehringer Ingelheim Fonds to P.J. Rauch; and the Korea Research Foundation Grant (KRF-2009-013-E00027) to W.W. Lee.

The authors declare no competing financial interests.

Submitted: 18 May 2011

Accepted: 5 December 2011

REFERENCES

- Aoki, S., A. Nakagomi, K. Asai, H. Takano, M. Yasutake, Y. Seino, and K. Mizuno. 2010. Elevated peripheral blood mononuclear cell count is an independent predictor of left ventricular remodeling in patients with acute myocardial infarction. *J. Cardiol.* 10.1016/j.jcc.2010.10.003.
- Auffray, C., D. Fogg, M. Garfá, G. Elain, O. Join-Lambert, S. Kayal, S. Sarmacki, A. Cumano, G. Lauvau, and F. Geissmann. 2007. Monitoring of blood vessels and tissues by a population of monocytes with patrolling behavior. *Science*. 317:666–670. <http://dx.doi.org/10.1126/science.1142883>
- Auffray, C., D.K. Fogg, E. Narni-Mancinelli, B. Senechal, C. Trouillet, N. Saederup, J. Leemput, K. Bigot, L. Campisi, M. Abitbol, et al. 2009. CX3CR1+ CD115+ CD135+ common macrophage/DC precursors and the role of CX3CR1 in their response to inflammation. *J. Exp. Med.* 206:595–606. <http://dx.doi.org/10.1084/jem.20081385>
- Balbay, Y., H. Tikiz, R.J. Baptiste, S. Ayaz, H. Saşmaz, and S. Korkmaz. 2001. Circulating interleukin-1 beta, interleukin-6, tumor necrosis factor-alpha, and soluble ICAM-1 in patients with chronic stable angina and myocardial infarction. *Angiology*. 52:109–114. <http://dx.doi.org/10.1177/000331970105200204>
- Brugger, W., W. Möcklin, S. Heimfeld, R.J. Berenson, R. Mertelsmann, and L. Kanz. 1993. Ex vivo expansion of enriched peripheral blood CD34+ progenitor cells by stem cell factor, interleukin-1 beta (IL-1 beta), IL-6, IL-3, interferon-gamma, and erythropoietin. *Blood*. 81:2579–2584.
- Cheong, C., I. Matos, J.H. Choi, D.B. Dandamudi, E. Shrestha, M.P. Longhi, K.L. Jeffrey, R.M. Anthony, C. Kluger, G. Nchinda, et al. 2010. Microbial stimulation fully differentiates monocytes to DC-SIGN/CD209(+) dendritic cells for immune T cell areas. *Cell*. 143:416–429. <http://dx.doi.org/10.1016/j.cell.2010.09.039>
- Darzynkiewicz, Z., S. Bruno, G. Del Bino, W. Gorczyca, M.A. Hotz, P. Lassota, and F. Traganos. 1992. Features of apoptotic cells measured by flow cytometry. *Cytometry*. 13:795–808. <http://dx.doi.org/10.1002/cyto.990130802>
- Devaraj, N.K., E.J. Keliher, G.M. Thurber, M. Nahrendorf, and R. Weissleder. 2009. 18F labeled nanoparticles for in vivo PET-CT imaging. *Bioconjug. Chem.* 20:397–401. <http://dx.doi.org/10.1021/bc8004649>
- Dolbear, F., H. Gratzner, M.G. Pallavicini, and J.W. Gray. 1983. Flow cytometric measurement of total DNA content and incorporated bromodeoxyuridine. *Proc. Natl. Acad. Sci. USA*. 80:5573–5577. <http://dx.doi.org/10.1073/pnas.80.18.5573>
- Duncan, D.S., and S.D. Miller. 2011. CNS expression of B7-H1 regulates pro-inflammatory cytokine production and alters severity of Theiler's virus-induced demyelinating disease. *PLoS ONE*. 6:e18548. <http://dx.doi.org/10.1371/journal.pone.0018548>
- Evan, G.I., A.H. Wyllie, C.S. Gilbert, T.D. Littlewood, H. Land, M. Brooks, C.M. Waters, L.Z. Penn, and D.C. Hancock. 1992. Induction of apoptosis in fibroblasts by c-myc protein. *Cell*. 69:119–128. [http://dx.doi.org/10.1016/0092-8674\(92\)90123-T](http://dx.doi.org/10.1016/0092-8674(92)90123-T)
- Fogg, D.K., C. Sibon, C. Miled, S. Jung, P. Aucouturier, D.R. Littman, A. Cumano, and F. Geissmann. 2006. A clonogenic bone marrow progenitor specific for macrophages and dendritic cells. *Science*. 311:83–87. <http://dx.doi.org/10.1126/science.1117729>
- Frangogiannis, N.G., C.W. Smith, and M.L. Entman. 2002. The inflammatory response in myocardial infarction. *Cardiovasc. Res.* 53:31–47. [http://dx.doi.org/10.1016/S0008-6363\(01\)00434-5](http://dx.doi.org/10.1016/S0008-6363(01)00434-5)
- Geissmann, F., M.G. Manz, S. Jung, M.H. Sieweke, M. Merad, and K. Ley. 2010. Development of monocytes, macrophages, and dendritic cells. *Science*. 327:656–661. <http://dx.doi.org/10.1126/science.1178331>
- Gordon, S., and P.R. Taylor. 2005. Monocyte and macrophage heterogeneity. *Nat. Rev. Immunol.* 5:953–964. <http://dx.doi.org/10.1038/nri1733>
- Graeber, M.B. 2010. Changing face of microglia. *Science*. 330:783–788. <http://dx.doi.org/10.1126/science.1190929>
- Guerra, S., A. Leri, X. Wang, N. Finato, C. Di Loreto, C.A. Beltrami, J. Kajstura, and P. Anversa. 1999. Myocyte death in the failing human heart is gender dependent. *Circ. Res.* 85:856–866.
- Harisinghani, M.G., J. Barentsz, P.F. Hahn, W.M. Deserno, S. Tabatabaei, C.H. van de Kaa, J. de la Rosette, and R. Weissleder. 2003. Noninvasive detection of clinically occult lymph-node metastases in prostate cancer. *N. Engl. J. Med.* 348:2491–2499. <http://dx.doi.org/10.1056/NEJMoa022749>
- Helft, J., F. Ginhoux, M. Bogunovic, and M. Merad. 2010. Origin and functional heterogeneity of non-lymphoid tissue dendritic cells in mice. *Immunol. Rev.* 234:55–75. <http://dx.doi.org/10.1111/j.0105-2896.2009.00885.x>
- Issekutz, T.B., A.C. Issekutz, and H.Z. Movat. 1981. The in vivo quantitation and kinetics of monocyte migration into acute inflammatory tissue. *Am. J. Pathol.* 103:47–55.
- Johnston, R.B.J. Jr. 1988. Current concepts: immunology. Monocytes and macrophages. *N. Engl. J. Med.* 318:747–752. <http://dx.doi.org/10.1056/NEJM198803243181205>
- Leuschner, F., P. Panizzi, I. Chico-Calero, W.W. Lee, T. Ueno, V. Cortez-Retamozo, P. Waterman, R. Gorbato, B. Marinelli, Y. Iwamoto, et al. 2010. Angiotensin-converting enzyme inhibition prevents the release of monocytes from their splenic reservoir in mice with myocardial infarction. *Circ. Res.* 107:1364–1373. <http://dx.doi.org/10.1161/CIRCRESAHA.110.227454>
- Li, T.S., M. Takahashi, R. Suzuki, T. Kobayashi, H. Ito, A. Mikamo, and K. Hamano. 2006. Pravastatin improves remodeling and cardiac function after myocardial infarction by an antiinflammatory mechanism rather than by the induction of angiogenesis. *Ann. Thorac. Surg.* 81:2217–2225. <http://dx.doi.org/10.1016/j.athoracsur.2005.12.065>
- Libby, P. 2002. Inflammation in atherosclerosis. *Nature*. 420:868–874. <http://dx.doi.org/10.1038/nature01323>
- Liu, K., G.D. Victora, T.A. Schwickert, P. Guermonprez, M.M. Meredith, K. Yao, F.F. Chu, G.J. Randolph, A.Y. Rudensky, and M. Nussenzweig. 2009. In vivo analysis of dendritic cell development and homeostasis. *Science*. 324:392–397. <http://dx.doi.org/10.1126/science.1171243>
- Llodrá, J., V. Angeli, J. Liu, E. Trogan, E.A. Fisher, and G.J. Randolph. 2004. Emigration of monocyte-derived cells from atherosclerotic lesions characterizes regressive, but not progressive, plaques. *Proc. Natl. Acad. Sci. USA*. 101:11779–11784. <http://dx.doi.org/10.1073/pnas.0403259101>
- Luo, Y., H. Zhou, J. Krueger, C. Kaplan, S.H. Lee, C. Dolman, D. Markowitz, W. Wu, C. Liu, R.A. Reisfeld, and R. Xiang. 2006. Targeting tumor-associated macrophages as a novel strategy against breast cancer. *J. Clin. Invest.* 116:2132–2141. <http://dx.doi.org/10.1172/JCI27648>
- Maekawa, Y., T. Anzai, T. Yoshikawa, Y. Asakura, T. Takahashi, S. Ishikawa, H. Mitamura, and S. Ogawa. 2002. Prognostic significance of peripheral monocytosis after reperfused acute myocardial infarction: a possible role for left ventricular remodeling. *J. Am. Coll. Cardiol.* 39:241–246. [http://dx.doi.org/10.1016/S0735-1097\(01\)01721-1](http://dx.doi.org/10.1016/S0735-1097(01)01721-1)
- McKinstry, W.J., C.L. Li, J.E. Rasko, N.A. Nicola, G.R. Johnson, and D. Metcalf. 1997. Cytokine receptor expression on hematopoietic stem and progenitor cells. *Blood*. 89:65–71.
- Mitruka, B.M., and H.M. Rawnsley. 1977. Clinical biochemical and hematological reference values in normal experimental animals. Masson Pub. USA, pp.

- Moskowitz, M.A., E.H. Lo, and C. Iadecola. 2010. The science of stroke: mechanisms in search of treatments. *Neuron*. 67:181–198. <http://dx.doi.org/10.1016/j.neuron.2010.07.002>
- Nahrendorf, M., D.E. Sosnovik, P. Waterman, F.K. Swirski, A.N. Pande, E. Aikawa, J.L. Figueiredo, M.J. Pittet, and R. Weissleder. 2007a. Dual channel optical tomographic imaging of leukocyte recruitment and protease activity in the healing myocardial infarct. *Circ. Res.* 100:1218–1225. <http://dx.doi.org/10.1161/01.RES.0000265064.46075.31>
- Nahrendorf, M., F.K. Swirski, E. Aikawa, L. Stangenberg, T. Wurdinger, J.L. Figueiredo, P. Libby, R. Weissleder, and M.J. Pittet. 2007b. The healing myocardium sequentially mobilizes two monocyte subsets with divergent and complementary functions. *J. Exp. Med.* 204:3037–3047. <http://dx.doi.org/10.1084/jem.20070885>
- Nahrendorf, M., H. Zhang, S. Hembrador, P. Panizzi, D.E. Sosnovik, E. Aikawa, P. Libby, F.K. Swirski, and R. Weissleder. 2008. Nanoparticle PET-CT imaging of macrophages in inflammatory atherosclerosis. *Circulation*. 117:379–387. <http://dx.doi.org/10.1161/CIRCULATIONAHA.107.741181>
- Nahrendorf, M., D.E. Sosnovik, B.A. French, F.K. Swirski, F. Bengel, M.M. Sadeghi, J.R. Lindner, J.C. Wu, D.L. Kraitchman, Z.A. Fayad, and A.J. Sinusas. 2009a. Multimodality cardiovascular molecular imaging, Part II. *Circ. Cardiovasc. Imaging*. 2:56–70. <http://dx.doi.org/10.1161/CIRCIMAGING.108.839092>
- Nahrendorf, M., P. Waterman, G. Thurber, K. Groves, M. Rajopadhye, P. Panizzi, B. Marinelli, E. Aikawa, M.J. Pittet, F.K. Swirski, and R. Weissleder. 2009b. Hybrid in vivo FMT-CT imaging of protease activity in atherosclerosis with customized nanosensors. *Arterioscler. Thromb. Vasc. Biol.* 29:1444–1451. <http://dx.doi.org/10.1161/ATVBAHA.109.193086>
- Nahrendorf, M., E. Keliher, B. Marinelli, P. Waterman, P.F. Feruglio, L. Fexon, M. Pivovarov, F.K. Swirski, M.J. Pittet, C. Vinegoni, and R. Weissleder. 2010a. Hybrid PET-optical imaging using targeted probes. *Proc. Natl. Acad. Sci. USA*. 107:7910–7915. <http://dx.doi.org/10.1073/pnas.0915163107>
- Nahrendorf, M., M.J. Pittet, and F.K. Swirski. 2010b. Monocytes: protagonists of infarct inflammation and repair after myocardial infarction. *Circulation*. 121:2437–2445. <http://dx.doi.org/10.1161/CIRCULATIONAHA.109.916346>
- National Heart, Lung, and Blood Institute. NHLBI Financial Year 2009 Factbook. http://www.nhlbi.nih.gov/about/FactBook2009_final.pdf
- Orelino, C., M. Peeters, E. Haak, K. van der Horn, and E. Dzierzak. 2009. Interleukin-1 regulates hematopoietic progenitor and stem cells in the midgestation mouse fetal liver. *Haematologica*. 94:462–469. <http://dx.doi.org/10.3324/haematol.13728>
- Panizzi, P., F.K. Swirski, J.L. Figueiredo, P. Waterman, D.E. Sosnovik, E. Aikawa, P. Libby, M. Pittet, R. Weissleder, and M. Nahrendorf. 2010. Impaired infarct healing in atherosclerotic mice with Ly-6C(hi) monocytosis. *J. Am. Coll. Cardiol.* 55:1629–1638. <http://dx.doi.org/10.1016/j.jacc.2009.08.089>
- Qiu, J., M. Nishimura, Y. Wang, J.R. Sims, S. Qiu, S.I. Savitz, S. Salomone, and M.A. Moskowitz. 2008. Early release of HMGB-1 from neurons after the onset of brain ischemia. *J. Cereb. Blood Flow Metab.* 28:927–938. <http://dx.doi.org/10.1038/sj.jcbfm.9600582>
- Robbins, C.S., and F.K. Swirski. 2010. The multiple roles of monocyte subsets in steady state and inflammation. *Cell. Mol. Life Sci.* 67:2685–2693. <http://dx.doi.org/10.1007/s00018-010-0375-x>
- Roger, V.L., A.S. Go, D.M. Lloyd-Jones, R.J. Adams, J.D. Berry, T.M. Brown, M.R. Carnethon, S. Dai, G. de Simone, E.S. Ford, et al. 2011. Executive Summary: Heart Disease and Stroke Statistics—2011 Update: A Report From the American Heart Association. *Circulation*. 123:459–463. <http://dx.doi.org/10.1161/CIR.0b013e3182009701>
- Serbina, N.V., and E.G. Pamer. 2006. Monocyte emigration from bone marrow during bacterial infection requires signals mediated by chemokine receptor CCR2. *Nat. Immunol.* 7:311–317. <http://dx.doi.org/10.1038/ni1309>
- Shimura, S., G. Yang, S. Ebara, T.M. Wheeler, A. Frolov, and T.C. Thompson. 2000. Reduced infiltration of tumor-associated macrophages in human prostate cancer: association with cancer progression. *Cancer Res.* 60:5857–5861.
- Spencer, S.L., and P.K. Sorger. 2011. Measuring and modeling apoptosis in single cells. *Cell*. 144:926–939. <http://dx.doi.org/10.1016/j.cell.2011.03.002>
- Swirski, F.K., M. Nahrendorf, M. Etzrodt, M. Wildgruber, V. Cortez-Retamozo, P. Panizzi, J.L. Figueiredo, R.H. Kohler, A. Chudnovskiy, P. Waterman, et al. 2009. Identification of splenic reservoir monocytes and their deployment to inflammatory sites. *Science*. 325:612–616. <http://dx.doi.org/10.1126/science.1175202>
- Swirski, F.K., M. Wildgruber, T. Ueno, J.L. Figueiredo, P. Panizzi, Y. Iwamoto, E. Zhang, J.R. Stone, E. Rodriguez, J.W. Chen, et al. 2010. Myeloperoxidase-rich Ly-6C⁺ myeloid cells infiltrate allografts and contribute to an imaging signature of organ rejection in mice. *J. Clin. Invest.* 120:2627–2634. <http://dx.doi.org/10.1172/JCI42304>
- Tacke, F., F. Ginhoux, C. Jakubzick, N. van Rooijen, M. Merad, and G.J. Randolph. 2006. Immature monocytes acquire antigens from other cells in the bone marrow and present them to T cells after maturing in the periphery. *J. Exp. Med.* 203:583–597. <http://dx.doi.org/10.1084/jem.20052119>
- Takemura, G., M. Ohno, Y. Hayakawa, J. Misao, M. Kanoh, A. Ohno, Y. Uno, S. Minatoguchi, T. Fujiwara, and H. Fujiwara. 1998. Role of apoptosis in the disappearance of infiltrated and proliferated interstitial cells after myocardial infarction. *Circ. Res.* 82:1130–1138.
- Tsujioka, H., T. Imanishi, H. Ikejima, A. Kuroi, S. Takarada, T. Tanimoto, H. Kitabata, K. Okochi, Y. Arita, K. Ishibashi, et al. 2009. Impact of heterogeneity of human peripheral blood monocyte subsets on myocardial salvage in patients with primary acute myocardial infarction. *J. Am. Coll. Cardiol.* 54:130–138. <http://dx.doi.org/10.1016/j.jacc.2009.04.021>
- van Furth, R., and Z.A. Cohn. 1968. The origin and kinetics of mononuclear phagocytes. *J. Exp. Med.* 128:415–435. <http://dx.doi.org/10.1084/jem.128.3.415>
- Weissleder, R., K. Kelly, E.Y. Sun, T. Shtatland, and L. Josephson. 2005. Cell-specific targeting of nanoparticles by multivalent attachment of small molecules. *Nat. Biotechnol.* 23:1418–1423. <http://dx.doi.org/10.1038/nbt1159>